This article has been accepted for publication in IEEE Journal on Flexible Electronics. This is the author's version which has not been fully edited and content may change prior to final publication. Citation information: DOI 10.1109/JFLEX.2026.3698890

Flexible β - Phase PVDF-Cu-MAA Self-Powered Nanofiber Nanogenerator for Energy Harvesting Applications

Sachin[1] Student Member IEEE, Sumit Choudhary[2*], Senior Member IEEE, and Satinder K. Sharma[1*], Senior Member IEEE

Abstract - This work reports the efficient development of polyvinylidene fluoride (PVDF) nanofibers doped with copper methacrylate (Cu-MAA) to form metal-organic clusters (MOCs), demonstrating notable energy generation and harvesting capabilities, and having strong potential for flexible electronics applications. A flexible piezoelectric nanogenerator (PENG) device was fabricated using electrospun PVDF-Cu-MAA nanofibers. These nanofibers form a matrix embedded between two flexible electrodes to fabricate device structures capable of converting mechanical force into electrical energy, and thereby enabling self-powered sensing. The pristine PVDF-based PENG devices and PVDF-Cu-MAA hybrid PENG devices produced a peak-to-peak output voltage of approximately 2.14V and 6.14V under mechanical tapping, respectively. The incorporation of 5 w/v% Cu-MAA significantly improved the piezoelectric response without compromising the flexibility of the polymer mat. These enhancements are primarily attributed to the increased formation of the polar β-phase in the hybrid nanofibers. Furthermore, the PENG devices were integrated with a DHT11 sensor and EPS-32 microcontroller, enabling real-time temperature and humidity sensing. These findings demonstrate the high potential of Cu-MAA-doped PVDF hybrid nanofibers PENG device for use in self-powered energy harvesting systems and sustainable sensing applications.

***Index Terms*— Electrospinning, piezo electric nano generators (PENGs), polyvinylidene fluoride (PVDF), Cu-MAA, Metal-organic clusters (MOCs), Self-powered sensor, ESP-32, Temperature, Humidity.**

The date of submission 08 March, 2026,

Sachin[1] and Satinder K. Sharma[1]* are with the School of Computing and Electrical Engineering, Indian Institute of Technology (IIT), Mandi, Himachal Pradesh, 175005, India. (e-mail*: satinder@iitmandi.ac.in)

Sumit Choudhary[2]* are with Department of Engineering and Technology, Gurugram University, Gurugram, 122023, India (e-mail*: sumit@gurugramuniversity.ac.in).

I. INTRODUCTION

WITH the rapid development of mobile and portable electronics, there is a growing need to find sustainable energy sources to power these low-power portable gadgets. Currently, the major approach for powering these electronics with the use of energy storage units like rechargeable batteries[1]. However, the main drawback of these energy storage units is that they require frequent recharging, have a limited lifespan, and therefore cannot be used to power portable gadgets indefinitely. Alternatively, such low-power devices can be powered sustainably by harvesting and utilizing ubiquitous small-scale ambient energy sources. In recent times, the nanogenerators based on piezoelectric, pyroelectric, and triboelectric phenomena have been significantly studied and researched to harvest energy from the ambient environment[2]. In contrast to piezoelectric ceramics like lead Potassium Niobate ($KNbO_3$), Lithium Niobate ($LiNbO_3$), Zinc oxide (ZnO), and Barium Titanate ($BaTiO_3$), ferroelectric polymers such as polyvinylidene fluoride (PVDF) and its copolymers have shown significant potential for piezoelectric nanogenerator applications. However, due to the toxicity, hazardous nature in livelihood, and non-flexibility of ceramic materials, these materials are restricted in routine daily life applications. So, nowadays, researchers are taking more interest in developing polymer-based piezoelectric nanogenerators because of their flexibility. Among various types of piezo-polymers, PVDF is mostly preferred because of its excellent piezoelectric features[3].Meanwhile, Cu-MOCs, like other MOCs, exhibit a highly porous structure with tunable pore sizes and high surface area, which makes them suitable for a wide range of applications such as energy storage, catalysis, gas storage, photocatalysis, sensing, and drug delivery [4] Cu-based MOCs exhibit excellent coordination flexibility, allowing the formation of stable frameworks with tunable structures and high surface area in the nanofibers. In addition, copper possesses favorable interaction with organic ligands, which contribute to enhanced electrical polarization, and dielectric behavior. Copper is comparatively low-cost, readily available, and compatible with facile solution-based synthesis routes, making Cu-MOCs attractive for scalable electronic and sensing applications as reported in previous studies also[5][6].

The mechanism behind the operation of PENG devices is the generation of electrical signals through contact electrification, which occurs due to repeated contact and separation. The PENG device's structures possess easy design, cost effectiveness, and compactness, making PENGs suitable for energy harvesting and to run low-power devices[7], [8]. Moreover, most previous research has mainly highlighted the PENG output performance under external load conditions, whereas few research studies have explored the process of utilizing a PENG device to concurrently run the load and charge an energy storage unit to power the load during the inactive

period. For performance enhancement in the piezoelectric PVDF nanofibers, achieving higher fractions of electroactive crystalline phases, particularly the β-phase, which exhibits the highest spontaneous polarization is critical [9][10]. Various methods, including spin-coating, casting, mechanical stretching, electrical poling and electrospinning offer scalability and simplicity in activating the electroactive β-phase [11]. During electrospinning under an applied high electric field, the simultaneous alignment of CH_2/-CF_2 molecular dipoles in PVDF-Cu-MAA occurs, during electrospinning.

Therefore, electrospun PVDF-Cu-MAA hybrid nanofibers demonstrate remarkable piezoelectric properties without the requirement of post-electrical poling.The piezoelectric response of PVDF-based nanofibers may be further enhanced through the incorporation of nanofillers and doping, as demonstrated by previous studies [12][13] . For instance, the introduction of 5 (w/v%) Cu-MAA MOCs into PVDF nanofibers results in an enhancement in piezoelectric response. The inclusion of MOCs, such as Cu-MAA, is theorized to improve the crystalline phase, thereby amplifying the piezoelectric response. MOCs have also proven effective in enhancing the piezoelectric characteristics of PVDF-based nanofibers through polar interactions between PVDF chains and the functional groups of the dopants [14]. Recent investigations have identified improved energy generation through the incorporation of Cu-MAA MOCs mixtures [15].

In the current study, we describe a self-powering piezoelectric sensor that harvests energy and uses it to power a microcontroller integrated with an environmental monitoring sensor (DHT11). The graphical abstract of the work is presented in Fig. 1. The nanofiber PVDF membrane was fabricated using a horizontal electrospinning equipment. Cu-MAA MOCs was added to the PVDF polymer solution to enhance β-phase crystallinity. As the concentration of MOCs increased, the fiber diameter decreased while the β-phase content increased. As a result, a PENG device with a high output voltage (6.14V) is developed. The impact of the MOCs inclusion in PVDF nanofibers is discussed and presented. The PVDF and MOCs hybrid nanofibers are used to harness energy and power a microcontroller (ESP32) and an environmental monitoring sensor (DHT11) [16], [17].

II. Experimental

A. Synthesis of Copper-Metal-Organic Cluster

Materials used were Polyvinylidene fluoride (1,80000 gpc), Dimethylformamide (73.09 g/mol), Cu-Acetate (199.65g/mol), Ethyl-Acetate (88.11 g/mol), Methacrylic Acid (86.09g/mol), Triethyl Amine (101.19g/mol), and Toluene (92.14g/mol) obtained from Sigma Aldrich. Initially, mixture was first prepared by dissolving 1 g of copper acetate hydrate in 40 mL of ethyl acetate under magnetic stirring to form solution A. Separately, solution B was prepared by mixing 2 g of methacrylic acid (MAA) with 1.8 g of trimethylamine. Solution B was then added dropwise to solution A under continuous stirring to enable controlled reaction and proper coordination for forming Cu-MOCs. Afterward, the mixture was placed in an oven at 60 °C for another 24 hours to slowly evaporate the solvent and promote crystal formation of Cu–MOCs at the bottom. The product was then washed with toluene to remove impurities and residual reagents. Finally, the material was dried at 50 °C to get the final product.

B. Solution Preparation and Electrospinning.

PVDF pellets were dissolved in a solvent mixture containing 24 w/v% PVDF, 56 w/v% DMF, and 20 w/v% acetone, followed by stirring for 6 hours at 75 °C. Cu-MOCs at 1 and 5 w/v% were added, and the mixture was sonicated for 2 hours to ensure uniform dispersion. A flexible ITO-coated PET sheet was cleaned using soap water, then sonicated in DI water and IPA. For electrospinning, the prepared PVDF and PVDF–Cu-MOCs solutions were loaded into a 2.5 mL syringe with a 9.8 mm needle. A 15 kV DC voltage was applied to the needle, while the ITO-PET substrate was placed on a grounded aluminum plate. Electrospinning was carried out using a horizontal E-spin instrument at a 13 cm distance from the rotating collector and a 0.8 µL/s flow rate. Nanofibers from pure PVDF and Cu-MOC-incorporated solutions were deposited onto the ITO-PET sheet, forming uniform fibrous membranes.

C. Morphological, Piezoresponse Force Microscopy (PFM) & Tensile Strength Characterizations

Scanning electron microscope (SEM) and Energy Dispersive X-ray Spectroscopy (EDS) mapping were acquired using a field emission SEM (FE-SEM) (Zeiss Gemini 500, Carl Zeiss Microscope) using an acceleration voltage of 5-kV. AFM (Bruker Dimension Icon) was used to analyze PVDF and PVDF–Cu-MAA nanofibers transferred onto a gold-coated silicon wafer, with the gold layer grounded for PFM measurements. A 10 nm conductive probe (spring constant 3 N/m, resonant frequency 75 kHz) operated in contact mode. Amplitude–voltage and phase–voltage loops were measured using voltage ramps from + 12 to -12 V. Mechanical testing of Cu-MAA-incorporated electrospun PVDF nanofibers was performed using equal-sized mats (1×6 cm^2). Tensile strength and stress–strain curves were measured on a Tinius Olsen UTM using a 10 N load cell, 3 cm gauge length, and 1 mm/min strain rate.

D. Structural and Spectroscopic Analysis

Raman spectroscopy was performed using a LabRAM HR Evolution system with a 532 nm laser, 50X objective, and 1800 gr/mm grating. The crystallinity was analyzed by XRD (Smart Lab Diffractometer) at a 1°/min scan rate.

III. Results and Discussion

A. Size and Morphology of Nanofiber

Fig. 2 presents FE-SEM micrographs of

This article has been accepted for publication in IEEE Journal on Flexible Electronics. This is the author's version which has not been fully edited and content may change prior to final publication. Citation information: DOI 10.1109/JFLEX.2026.3698890

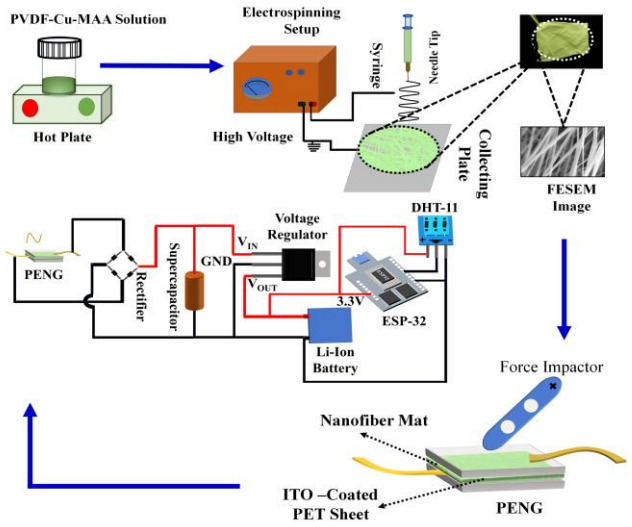

Fig. 1. Schematic diagram of process flow for the fabrication of electrospun PVDF-Cu-MAA MOCs nanofibers-based PENG device.

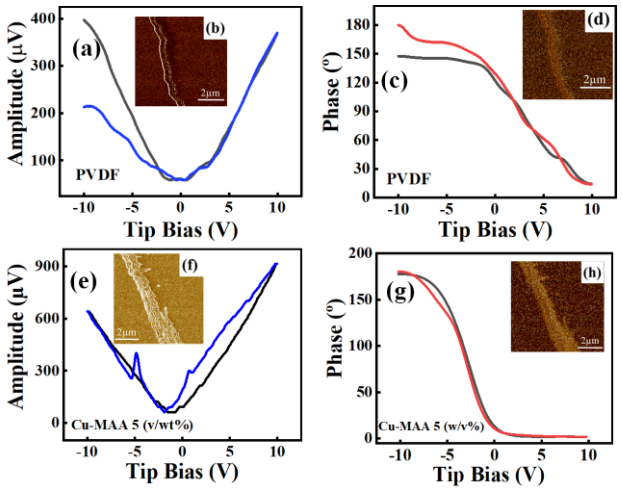

Fig. 3. PFM analysis of PVDF and PVDF–Cu-MAA (5 w/v%). (a, b) Amplitude vs. voltage curve and amplitude image of PVDF. (c, d) Phase vs. voltage curve and phase image of PVDF. (e, f) Amplitude vs. voltage curve and amplitude image of PVDF–Cu-MAA (5 w/v%). (g, h) Phase vs. voltage curve and phase image of PVDF–Cu-MAA (5 w/v%).

Polyvinylidene fluoride (PVDF) and PVDF-Cu-MAA hybrid fibrous membranes. The micrographs display the size distribution of the fibers, along with the elemental analysis. In the case of PVDF, the electrospun nanofibers exhibit a bead-free and uniform morphology with an average diameter of approximately 100 nm. The effective elemental incorporation of Cu-MAA MOCs doped PVDF nanofibers was further

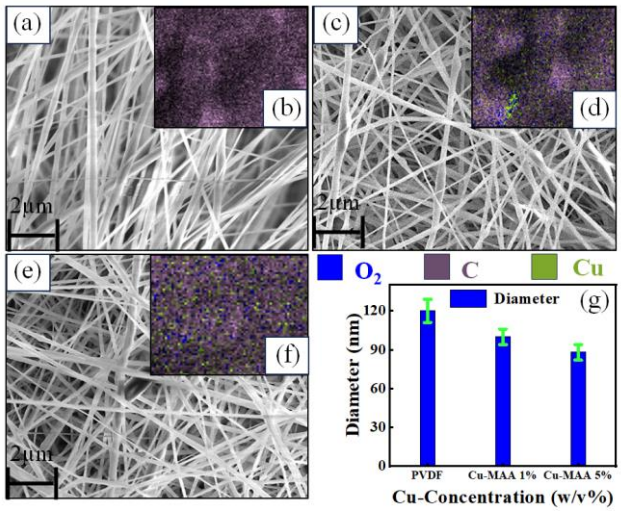

Fig. 2. (a, c, e) FESEM micrographs of PVDF-Cu-MAA hybrid nanofibers at various Cu-MAA concentrations. Inset (d, e, f) EDS area mapping of the nanofibers. (g) Average size of the nanofibers at different Cu-MAA concentrations.

confirmed by EDS analysis, as illustrated in Inset Fig. 2 (b,d,f). Moreover, the DMF (Dimethylformamide) solvent used during the synthesis of the nanofibers has high volatility, which consequently helps to decorate the Cu-MAA MOCs at the outer shell of the fibres during the electrospinning and drying stages. Due to its rapid evaporation rate, a concentration gradient is generated along the fibre axis, driving the migration of the Cu-MAA clusters toward the fibre surface before solidification. This preferential outward movement promotes a surface-rich distribution of the MOCs rather than a uniform bulk embedding. A similar phenomenon has also been observed in previous studies [18]. Overall, inclusively, the micrographs and elemental analysis presented in Fig. 2 provide crucial insights into the electrospun nanofibers. Further, the morphology and composition of both the PVDF and PVDF-Cu-MAA hybrid fibrous matrix were characterised by the SEM analysis and EDS mapping, respectively.The results reveal the successful incorporation of Cu-MAA MOCs into PVDF nanofibers and the improved fiber uniformity achieved through Cu-MAA incorporation. The EDS mapping results revealed uniform dispersion of various elements within the PVDF polymer matrix. Elements such as carbon (C), oxygen (O), and copper (Cu) were identified and mapped throughout the material.This confirmed the successful
incorporation and spatial distribution of Cu-MAA within the PVDF matrix.

B. PFM Analysis

Piezoresponse Force Microscopy (PFM) measures nanoscale piezoelectric response and structural orientation of ferroelectric and piezoelectric materials when an electric field is applied. PFM images show the topography, piezoelectric amplitude, and polarization distribution of a nanofiber when it is excited by an electric field. The amplitude PFM image contains areas with bright amplitude indicating that there is a large amplitude recorded due to a strong piezoelectric response and high spontaneous polarization; dark regions indicate that there is less of a response[19].The direction of the polarization can be determined from the phase contrast of the PFM image. Bright regions represent a dipole that is oriented upwards and dark regions represent a dipole that is oriented downwards. The resulting polarization maps provide information about the type of domains present, dipole alignment and electromechanical activity of the nanofibers. Comparison of hybrid PVDF-Cu-MAA (5 w/v%) nanofibers to pure PVDF fibers indicates a

This article has been accepted for publication in IEEE Journal on Flexible Electronics. This is the author's version which has not been fully edited and content may change prior to final publication. Citation information: DOI 10.1109/JFLEX.2026.3698890

significant difference in piezoelectric behavior between the two types of nanofibers as shown in Fig. 3. Hybrid nanofibers exhibit a distinct butterfly shaped amplitude hysteresis loop and a pronounced hysteresis in Piezoresponse Phase, including nearly 180° of phase shift indicating the ferroelectricity of the hybrid nanofibers Fig. 3 (e) [20]. The butterfly shaped hysteresis loop is caused by a nonlinear converse piezoelectric deformation that occurs during the polarization reversal and the hysteresis in Piezoresponse Phase indicates that the dipoles can be switched between two energetically stable dipole orientations, confirming a reversible domain switching in the hybrid nanofibers and measuring the resultant remanent polarization of the nanofibers demonstrating higher levels of ferroelectric order than that of the pristine PVDF fibers. Since the measurement was carried out on an individual nanofiber, local domain orientation and field distribution can also influence the unequal forward and reverse switching behavior observed in both amplitude and phase loops. Introducing Cu-MAA improves the ferroelectric characteristics of the polymer due to the localized electrostatic interactions and forms the basis for the creation of aligned dipoles, which enhances the degree of order within sample and increases the probability of formation of β-phase. The Cu-MAA also contributes to a conductive path for charge to travel used to create the internal pathways for conducting charge, reducing the internal resistance of the dipole and allowing for much more efficient movement of charge and thereby increasing electromechanical coupling factor and result in greater piezoelectricity.

C. Tensile Strength Analysis

Mechanical stability is a critical parameter for hybrid nanofibers intended for flexible energy harvesting devices. Fig. 4 (a) shows the stress–strain curves of pristine PVDF and PVDF-Cu-MAA hybrid nanofibers. It is clearly observed from the stress-strain curves that the PVDF-Cu-MAA hybrid nanofibers exhibit significantly higher tensile strength than the pristine PVDF nanofibers. Here, Cu-MAA acts as an effective nucleating agent, promoting β-phase crystallization and improving dipole chain alignment within the matrix[21]. These interfacial interactions facilitate efficient stress transfer, while the increased β-phase content enhances crystallinity and stiffness, together leading to the improved mechanical strength of the hybrid nanofibers [22]. The fracture points for pristine PVDF, PVDF-Cu-MAA, and PVDF-Cu-MAA (1, 5w/v%) nanofibers lie at ~4.4, ~9.2, and ~13.7 MPa, respectively, as illustrated in Fig. 4(b). This demonstrates that the strength of the PVDF-Cu-MAA hybrid nanofibers is higher than that of the pristine PVDF nanofibers. The enhanced strength and stiffness of the PVDF-Cu-MAA hybrid nanofibers can be attributed to the combined effect of the strong interface interaction between the Cu-MAA, MOCs, and the PVDF polymer. The estimated slope of the stress-strain curve, which yields the Young's modulus magnitudes, is 125.169 MPa, 146.007 MPa, and 192.339 MPa for PVDF, 1%(w/v) doped Cu-MAA MOCs and 5(w/v%) doped Cu-MAA MOCs into the PVDF, respectively[23]. These results clearly demonstrate that Cu-MAA doping enhances both tensile strength and elastic modulus, with the 5 w/v% sample exhibiting the most significant improvement. The PENG exhibits stable and repeatable voltage peaks during continuous 45° bending-release cycles, demonstrating strong mechanical durability and flexibility[24]. The consistent signal amplitude confirms efficient strain transfer and robust electromechanical coupling under tensile deformation as shown in Fig. 4 (c).

Additionally, the excellent tensile strength of the hybrid nanofibers results from the uniform dispersion within the polymer matrix and strong interfacial interactions of MOCs within the PVDF-Cu-MAA, hybrid matrix. Which exhibits the PVDF–Cu–MAA hybrid system, superior mechanical elasticity, making it a promising material for flexible and stretchable applications, particularly in PENG and TENG devices.

D. Piezoelectric Coefficient Analysis

The Piezoelectric coefficient value was measured using YE2730A, d_{33} Piezometer, (APC International, Ltd). The applied force to the nanofibers, 0.25N, is kept constant for all three set of device samples. It is observed that the d_{33} value of

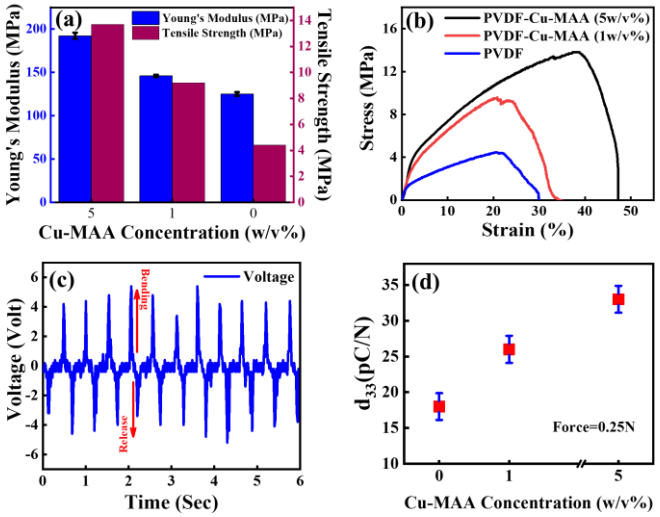

Fig. 4 (a) Stress–strain curves of PVDF, PVDF-Cu-MAA (1%), and PVDF-Cu-MAA(5%) nanofibers (b) Young Modulus and tensile strength of PVDF, PVDF-Cu-MAA (1%), and PVDF-Cu-MAA(5%) nanofibers (c) V-T curves at bending of device at angle of 45° (d) Piezoelectric coefficient (d33) of fabricated PVDF hybrid nanofibers corresponding to various concentrations (1,5 w/v%) of Cu-MAA MOCs.

PVDF nanofibers increases by incorporating the Cu-MAA, MOCs in the PVDF nanofibers matrix. The d_{33} coefficient increases from ~18 pC/N for pristine PVDF to 26 pC/N and 32 pC/N for the 1 and 5 w/v% Cu–MAA-loaded samples,corresponding to ~44% and ~78% enhancements, respectively. [42], [43]. The higher d_{33} value of the PVDF-Cu-MAA (1 w/v%) nanofibrous matrix was measured, which is significantly higher than that of the pristine, undoped sample as shown in Fig. 4 (d).

E. Structural and Spectroscopy Analysis

To further investigate and confirm that the enhanced polarization of PVDF-Cu-MAA fibers is due to induced β-phase, the Raman spectroscopy analysis of PVDF, and PVDF-Cu-MAA, 1 (w/v%), and 5 (w/v%) were carried out, & presented in Fig. 5 (a). The incorporation of Cu-MAA into the

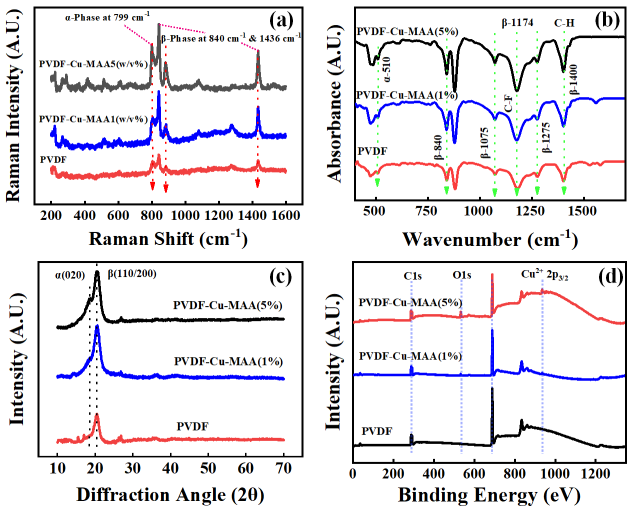

Fig. 5. (a) Raman analysis of PVDF, PVDF-Cu-MAA (1 w/v%) and PVDF-Cu-MAA(5 w/v%) nanofiber (b) FTIR analysis of PVDF, PVDF-Cu-MAA (1 w/v%) and PVDF-Cu-MAA (5 w/v%) nanofiber (c) XRD spectra of PVDF, PVDF - Cu-MAA(1 w/v%) PVDF - Cu-MAA(5 w/v%) (d) XPS analysis of PVDF, PVDF-Cu-MAA (1 w/v%) and PVDF-Cu-MAA(5 w/v%) nanofiber

PVDF matrix promotes β-phase formation because the Cu^{2+} ions and coordinated carboxylate functional groups generate strong local electrostatic fields and interfacial dipole–dipole interactions with the PVDF chains. These interactions disrupt the non-polar TGTG′ conformation of the α-phase and facilitate the transition toward the all-trans (TTTT) configuration, thereby stabilizing the β-phase during the electrospinning process[25]. The analysis of spectra of PVDF and PVDF-Cu-MAA systems shows two broad peaks at 799 cm^{-1} and 844 cm^{-1}, corresponding to the α-phase and β-phase, respectively [44]. The Raman spectra of electrospun PVDF-Cu-MAA show that the strength of the peak at 799 cm^{-1}, associated with the α phase, has decreased dramatically, but the peak at 844 cm^{-1}, associated with the β phase, has increased significantly. Further, the ratio of α and β signal intensity is utilized to find the relation between the two Raman peaks, using the following equation as given below: Where I_{844}, I_{799} and I_{1436} represent the absorbance value at (844 cm^{-1}), and (799 cm^{-1}, 1436 cm^{-1}) depicting (α) and (β) phases respectively.

$$\frac{\beta}{\alpha} = \frac{I_{844}}{I_{799}} \qquad \text{.....1}$$

Using equation (1) the prevalence of the phases was determined. In the PVDF-Cu-MAA 5 (w/v%) sample, the ratio is (1.88) higher as compared to 1(w/v%) Cu-MAA (1.05) and pristine PVDF (1.02) samples, respectively. i.e. This confirmed that the β phase is more dominant in 5 w/v% of the Cu-MAA, hybrid systems [26],[27]. The enhanced ratio of β /α phases signifies the β phase dominance, which confirms the enhanced induced polarization of PVDF + Cu-MAA fibers, corresponding to increased piezoelectricity[28].

FTIR spectroscopy was employed to investigate the phase composition and molecular interactions in PVDF nanofibers doped with Cu-MAA MOC. The spectra Fig. 5b show prominent peaks of the β-phase, including a significant absorption band at 840 cm^{-1}, which corresponds to the C−F stretching vibration of the polar crystalline structure. Another

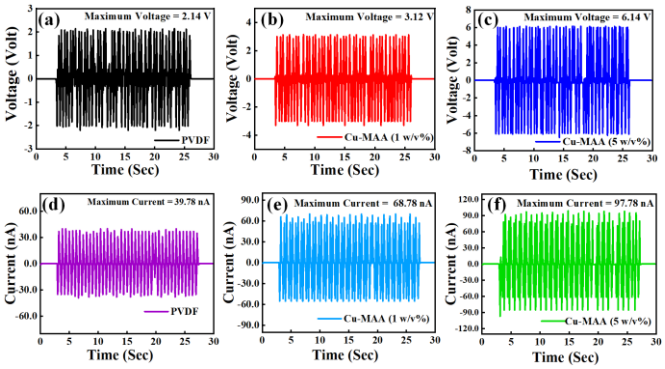

Fig. 6. V-T measurements with different concentration of Cu MOCs (a) Pristine PVDF, (b) PVDF-Cu-MAA (1w/v%) (c) PVDF-Cu-MAA(5w/v%). I-T measurement with different concentration of Cu MOCs (d) Pristine PVDF, (e) PVDF-Cu-MAA (1w/v%), (f) PVDF-Cu-MAA(5w/v%).

peak at 1400 cm^{-1} demonstrates the significant β-phase. Meanwhile, the α-phase peak around 1174 cm^{-1} is comparably less prominent. PVDF-Cu-MAA (5 w/v%) nanofibers exhibit markedly increased β-phase intensity, indicating strong interactions between Cu-MAA MOCs and PVDF chains. Localized electric fields produced by interactions between MOCs and PVDF atoms facilitate the alignment of dipoles in polymer chains, stabilising the β-phase and enhancing piezoelectric properties[29]. The FTIR spectra confirm that Cu-MAA doping significantly alters the structural properties of PVDF nanofibers, promoting the stabilisation of the β-phase and enhancing piezoelectric responsiveness.

The polymorphism of the PVDF-Cu-MAA nanofibers was further examined by analysing, X-ray diffraction (XRD) spectra, as illustrated in Fig. 5 (c). Different crystalline peaks can be seen in the PVDF nanofibers XRD pattern; the most noticeable peak is located in the 2θ range at about 20.3°, Fig. 5(c). The XRD spectra of Cu-MAA (1,5 w/v%) doped nanofibers and pure PVDF are shown in Fig. 5c.

In pristine PVDF nanofibers, a dominant diffraction peak at 2θ ≈ 20.3° corresponds to the (110)/(200) planes of the β-phase, which is caused by Bragg diffraction from the crystalline β-phase's 110/200 planes. In the 2θ range, the nonpolar α-phase (020) at approximately 18.5° appears not to be very prominent. I_α and I_β refer to the diffraction peak intensities for the α- and β-phases, respectively. Cu-MAA doping (5 w/v%) enhanced the β-phase content (I_β = 9096.99), indicating an improved development of the polar crystalline β-phase, whereas pristine PVDF nanofibers showed a β-phase (I_β = 4990.67). In comparison to pristine PVDF nanofibers, the XRD spectrum of doped nanofibers with an optimal Cu-MAA concentration (5 w/v%) exhibited a notable increase in peak strength correlating with the β-phase[30]. To enhance the piezoelectric performance in energy harvesting devices, these results demonstrate that Cu-MAA doping significantly increases the β-phase content in PVDF-Cu-MAA nanofibers. The XPS scan and high-resolution spectra demonstrate that Cu-MAA MOCs were successfully incorporated into the PVDF matrix at 1 and 5 wt%. The F 1s peak at 688.3 eV, typical of C-F/CF_2 groups, shows that the PVDF backbone is still intact after doping. The C 1s peak at 286.37 eV exhibits increased C-C/C-F and O-C=O ligands and improved PVDF-Cu-MAA interfacial interactions[31]. The

O1s signal at 532.19 eV shows coordination between Cu^{2+} and MAA ligand, indicating Cu-O-C and C=O species. Satellites confirm the Cu $2p_{3/2}$ signal at 935.07 eV, indicating the retention of Cu^{2+} oxidation state. The 1% and 5% samples have higher O 1s and Cu 2p intensities, indicating larger cluster loading as shown in Fig. 5 (d).

F. Electrical Analysis

The output characteristics of the fabricated flexible PENG devices were thoroughly evaluated and analysed. The in-house designed and developed force impact transducer based on an Arduino microcontroller and servo motors, were used to apply a constant & consistent mechanical force on the PENG device. The programmed transducer continuously taps on the active device area with uniform force. The magnitude of force applied to the PENG is calculated by

$$F = \frac{r}{\tau} \qquad \ldots\ldots\ldots\ldots 2$$

where r =1.98 cm is the length of arm and τ = 10.5 kg/cm is the torque of the servo motor (MG996R). This setup ensured consistent loading conditions across all tests. The output signals were meticulously recorded using an Digital Storage Oscilloscope (DSO) make Agilent Technologies DSO1052B and Keithley SCS4200 characterization tool. Fig. 6 (a,b,c) portrays the different output voltages at different concentrations of Cu-MAA MOCs. The output voltage and current for the

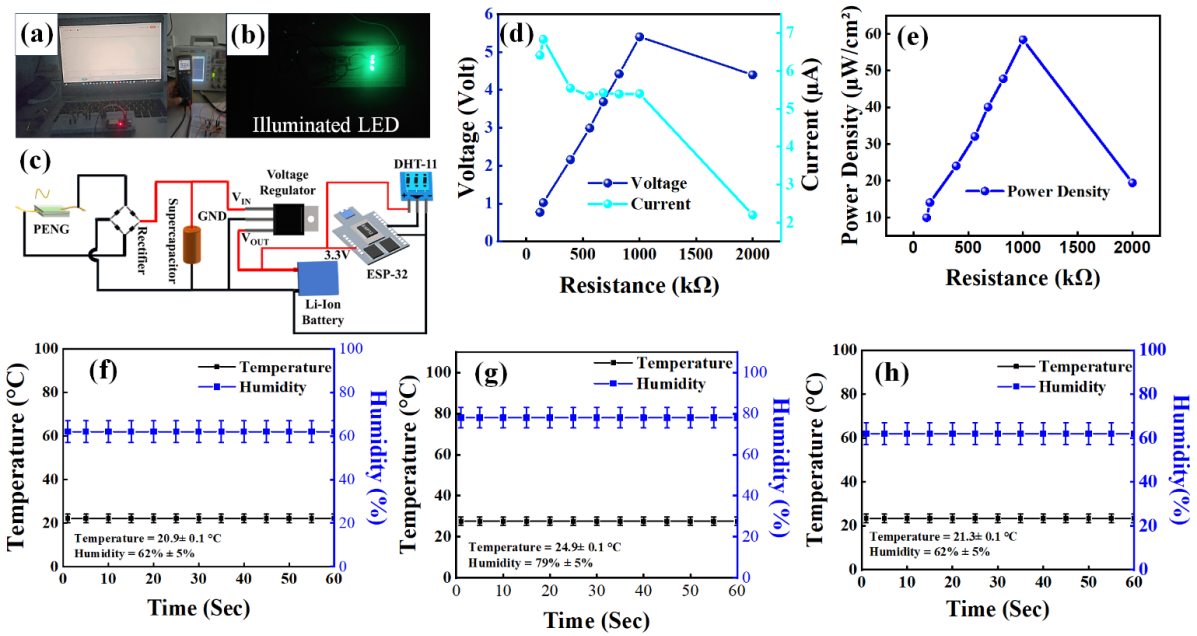

Fig. 7. (a,b) Illuminated LED and real-time charging of a capacitor using PENG (c) Schematic of the circuit used for energy harvesting. (d) Current vs Voltage at different loads (e) Power density at different loads. (f-h) Humidity and temperature at different environmental conditions (set a), (set b) and (set c), respectively.

pristine PVDF sample is 1.98 V and 39.78 nA. The measured output voltage and current are increasing with an increase in the concentration of Cu-MAA in the PVDF solution. For instance, in the 1w/v% PVDF-Cu-MAA samples, the measured voltage and current are 2.8V and 68.78nA, and for the PVDF-Cu-MAA (5w/v%) sample, the measured voltage and current are 6.14V and 97.78nA, respectively. The PVDF-Cu-MAA (5 w/v%) PENG devices demonstrated a maximum output voltage of approximately 6.14 V, which is attributed to the higher concentration of Cu-MAA in PVDF. The revealed results provide valuable insights into the influence of MOCs concentration on the device's piezoelectric performance characteristics. Further, to characterize the current vs time (I-T) characteristics of the PENG devices at different concentrations of Cu-MAA MOCs. Fig. 6 (d,e,f) illustrates the different output I-T characteristics at different concentrations of Cu-MAA MOCs. Remarkably, the PENG devices demonstrated a maximum output current of approximately 97.78 nA, with a Cu-MAA 5(w/v%) MOCs. Furthermore, evaluate the device's maximum current density of Cu-MAA, with 5 w/v% MOCs was around 0.196 μA/cm^2. The enhanced electrical output correlates directly with the increased β-phase fraction induced by Cu-MAA doping. The Cu^{2+} carboxylate coordination promotes an all-trans chain conformation, resulting in higher spontaneous polarization and improved dipole alignment within the polymer matrix. This structural ordering increases the effective piezoelectric coefficient and reduces dielectric loss, enabling greater charge separation under mechanical excitation. As a result, the Cu-MAA-induced β-phase contributes to stronger electromechanical coupling and yields a significantly amplified voltage and current response compared to pristine PVDF.

The output characteristics of the PENG were evaluated across varying external load resistances. As resistance increases, the voltage gradually rises while the current decreases, consistent with the internal impedance behavior of the device. The power density exhibits a clear maximum around ~1 MΩ, indicating optimal load matching for maximum energy extraction as shown in Fig. 7 (b,c). This peak power density reflects efficient charge transfer and validates the device's capability for practical low-power applications.The measured results provide valuable insights into the influence of MOCs

concentration on the device's piezoelectric characteristics. To further investigate the feasibility of the fabricated PENG device in the real-time environment, the PENG device is used as a power source for running an ESP-32 low power processor equipped with DHT 11 temperature and humanity sensor. The temperature dependent study under elevated or reduced temperatures were also examined Fig. SI-4 Supplementry information (SI).The dielectric permittivity and conductivity of the films are observed to increase with the temperature. The increase in the dielectric permittivity has been attributed to the PVDF segmental chain's movements, causing the enhancement in dielectric permittivity, which results in more surface charge and improvements in the PENG electrical outputs. However, a large increment in film conductivity at higher temperatures causes the leakage of surface charges, resulting in a decrement in PENG outputs[32]. Furthermore, the device was continuously tested for 1500 sec under repeated mechanical stimulation, and a stable electrical output was observed in Fig. SI-3 (SI) throughout the measurement duration with negligible degradation.

To demonstrate the real-time application of the fabricated PENG devices. The generated alternating voltage signals from the PENG devices need to be conditioned to power the DC-powered ESP-32 microprocessor. To accomplish this, a bridge rectifier circuit is used in the first stage of the circuit to harness the DC component from the energy generated by the PENG devices. The bridge rectifier converts the AC input voltage to DC. The output from the bridge circuit was used to light the LEDs, confirming energy generation from the PENG device. Henceforth, to demonstrate the real-time temperature and humidity sensing application, the output from the bridge rectifier was connected in parallel with the supercapacitor (5.5V) and the voltage regulator to provide the necessary power to the EPS-32 microcontroller. Further the supercapacitor provides the accumulated energy to supply power to EPS-32 in real-time and simultaneously provide energy to charge the parallelly connected the Li-Ion battery, which acts as a constant power source for the microcontroller, the connected Li-Ion battery not only provides the constant power source but also provides power to the EPS-32 during short in-active periods, when no stimulus applied to the PENG device mat. The fabricated PENG devices demonstrated effective charging of the supercapacitor and powered the ESP microprocessor. Fig. 7(b). illustrates the real-time charging and discharging of a capacitor while simultaneously powering an ESP 32 equipped with a DHT 11 sensor, which shows real-time monitoring of the temperature and humidity.

The ESP processor, integrated with a humidity sensor, was used to monitor different environmental conditions in real-time. The different locations were chosen to have varied temperature and humidity conditions, which will not only test the device in real-time but also assess its reliability under distinct conditions. Three set of environmental conditions were chosen within our laboratory locations such as set (a) with temperature of 23.4 °C (±2°C) and humidity is 78% (±5%), set (b) with temperature and humidity 22.1 4 °C (±2°C) and 62 % (±5%) and set (c) measured at a closed room environment with temperature 23.4 °C (±2°C) and humidity 62% (±5%). These parameters were recorded by our prototype devices as depicted in Fig. 7 (f,g,h) and were also cross-checked with a commercially available standard sensor. The sustained and continuous mechanical impacts are sufficient to continuously power the EPS-32 board which is illustrated by the glowing embedded on-board LEDs of EPS-32 motherboard. The supercapacitor is capable of delivering the power up to 5 sec upon continuous beating after the cessation of mechanical beating, for longer inactive intervals (>5 sec) ESP-32 draws power from the parallel-connected Li-ion battery. When the ESP-32 is in standby mode, the continuous beating enables Li-ion battery charging. These demonstrations affirm that the PENG device efficiently converts the mechanical energy into electrical energy, enabling the effective powering of small, low-power systems. Additionally, the energy output can be further enhanced by increasing the PENG area or by stacking multiple PENG in a series and parallel configuration. Thus, the PENG presented in this study emerges as a promising device for portable and self-powered next-generation devices.

IV. Conclusion

In conclusion, this research has successfully developed and characterized a flexible piezoelectric nanogenerator based on electrospun PVDF-Cu-MAA nanofibers for energy harvesting applications.Comprehensive characterization confirmed the device's performance, including a high piezoelectric coefficient (d_{33}), significant output voltage (~6.14 V), and efficient current density (~0.196 μA/cm²). The fabricated devices were further validated in a real-time demonstration, successfully powering a temperature and humidity sensing system (ESP32 + DHT11), thereby highlighting its ability to effectively harvest mechanical energy and convert it into usable electrical power. Overall, the incorporation of Cu-MAA into PVDF nanofibers has been shown to stabilize the electroactive β-phase, improve polarization alignment, and enhanced electrical output. These findings enable the development of self-powered, energy-efficient nanogenerators suitable for IoT devices, wearables, and future autonomous sensor networks.

Acknowledgments

The authors greatfully acknowledge the Centre for Design and Fabrication of Electronic Devices (C4DFED), Advanced Materials Research Centre (AMRC), Indian Institute of Technology (IIT) Mandi, India for providing state-of-the-art device fabrication and characterization facilities for this work.

References

[1] Y. W. Chong, W. Ismail, K. Ko, and C. Y. Lee, "Energy Harvesting for Wearable Devices: A Review," *IEEE Sens. J.*, vol. 19, no. 20, pp. 9047–9062, Oct. 2019, doi: 10.1109/JSEN.2019.2925638.

[2] B. Chen *et al.*, "Flexible piezoelectrics: integration of sensing, actuating and energy harvesting," Dec. 01, 2025, *Nature Research*. doi: 10.1038/s41528-025-00432-5.

[3] L. Persano *et al.*, "High performance piezoelectric devices based on aligned arrays of nanofibers of poly(vinylidenefluoride-co-trifluoroethylene)," *Nat. Commun.*, vol. 4, 2013, doi: 10.1038/ncomms2639.

[4] R. Kumar, M. Chauhan, M. G. Moinuddin, S. K. Sharma, and K. E. Gonsalves, "Development of Nickel-Based Negative Tone Metal Oxide Cluster Resists for Sub-10 nm Electron Beam and Helium Ion Beam Lithography," *ACS Appl. Mater. Interfaces*, vol. 12, no. 17, pp. 19616–19624, Apr. 2020, doi: 10.1021/acsami.9b21414.

[5] P. Chandra *et al.*, "Copper-Based Metal-Organic Frameworks for Sustainable Catalysis: Mechanistic Insights, Stability, and Emerging

Research Directions.," *ACS Omega*, vol. 11, no. 6, pp. 8911–8939, Feb. 2026, doi: 10.1021/acsomega.5c10345.

[6] P. Gupta, R. Kumar, and S. K. Sharma, "Integration of High-Performance Cost-Effective Copper-Metal-Organic-Nanocluster-based Gate Dielectric for Next-Generation CMOS Applications," *Adv. Electron. Mater.*, vol. 7, no. 4, Apr. 2021, doi: 10.1002/aelm.202000835.

[7] M. Abbasipour, R. Khajavi, and A. H. Akbarzadeh, "A Comprehensive Review on Piezoelectric Polymeric and Ceramic Nanogenerators," Jun. 01, 2022, *John Wiley and Sons Inc*. doi: 10.1002/adem.202101312.

[8] S. Bano, P. Sahdev, G. Kumar, S. Choudhary, and R. Singh, "Conducting Gel-Assisted Triboelectric Sensor Array for Self-Powered Wireless Pressure Distribution and Emergency Alert System," *IEEE Sens. J.*, pp. 1–1, Jan. 2026, doi: 10.1109/jsen.2026.3651863.

[9] P. Martins, A. C. Lopes, and S. Lanceros-Mendez, "Electroactive phases of poly(vinylidene fluoride): Determination, processing and applications," 2014, *Elsevier Ltd*. doi: 10.1016/j.progpolymsci.2013.07.006.

[10] H. Varghese, B. S. Athira, and A. Chandran, "Highly Flexible Triboelectric Nanogenerator Based on PVDF Nanofibers for Biomechanical Energy Harvesting and Telerehabilitation via Human Body Movement," *IEEE Sens. J.*, vol. 23, no. 13, pp. 13925–13932, Jul. 2023, doi: 10.1109/JSEN.2023.3271663.

[11] J. E. Lee, Y. Eom, Y. E. Shin, S. H. Hwang, H. H. Ko, and H. G. Chae, "Effect of Interfacial Interaction on the Conformational Variation of Poly(vinylidene fluoride) (PVDF) Chains in PVDF/Graphene Oxide (GO) Nanocomposite Fibers and Corresponding Mechanical Properties," *ACS Appl. Mater. Interfaces*, vol. 11, no. 14, pp. 13665–13675, Apr. 2019, doi: 10.1021/acsami.8b22586.

[12] H. Parangusan, D. Ponnamma, and M. Al Ali Almaadeed, "Toward High Power Generating Piezoelectric Nanofibers: Influence of Particle Size and Surface Electrostatic Interaction of Ce-Fe 2 O 3 and Ce-Co 3 O 4 on PVDF," *ACS Omega*, vol. 4, no. 4, pp. 6312–6323, Apr. 2019, doi: 10.1021/acsomega.9b00243.

[13] B. Amrutha, A. Anand Prabu, and M. Pathak, "Enhancing piezoelectric effect of PVDF electrospun fiber through NiO nanoparticles for wearable applications," *Heliyon*, vol. 10, no. 7, Apr. 2024, doi: 10.1016/j.heliyon.2024.e29192.

[14] Y. Jiang *et al.*, "Unveiling Mechanically Driven Catalytic Processes: Beyond Piezocatalysis to Synergetic Effects," May 20, 2025, *American Chemical Society*. doi: 10.1021/acsnano.5c02660.

[15] J. C. Barbosa *et al.*, "Metal organic framework modified poly(vinylidene fluoride-co-hexafluoropropylene) separator membranes to improve lithium-ion battery capacity fading," *Chemical Engineering Journal*, vol. 443, Sep. 2022, doi: 10.1016/j.cej.2022.136329.

[16] S. Z. Hussain, V. P. Singh, M. S. Bin Sadeque, S. Yavari, G. Kalimuldina, and M. Ordu, "Piezoelectric-Triboelectric Hybrid Nanogenerator for Energy Harvesting and Self-Powered Sensing Applications," 2025, *John Wiley and Sons Inc*. doi: 10.1002/smll.202504626.

[17] M. Shekari, G. Naderi, S. Moghari, M. Naqvi, and H. A. Khonakdar, "Piezoelectric Materials for Energy Harvesting in Wearables," *Polym. Eng. Sci.*, Oct. 2025, doi: 10.1002/pen.70186.

[18] S. Kailasa, M. S. B. Reddy, M. R. Maurya, B. G. Rani, K. V. Rao, and K. K. Sadasivuni, "Electrospun Nanofibers: Materials, Synthesis Parameters, and Their Role in Sensing Applications," Nov. 01, 2021, *John Wiley and Sons Inc*. doi: 10.1002/mame.202100410.

[19] F. Calavalle, M. Zaccaria, G. Selleri, T. Cramer, D. Fabiani, and B. Fraboni, "Piezoelectric and Electrostatic Properties of Electrospun PVDF-TrFE Nanofibers and their Role in Electromechanical Transduction in Nanogenerators and Strain Sensors," *Macromol. Mater. Eng.*, vol. 305, no. 7, Jul. 2020, doi: 10.1002/mame.202000162.

[20] S. Verma, M. Sharma, and R. Vaish, "Photo-piezocatalysis in electrospun PVDF + WS2 membrane," *Environ. Sci. Nano*, vol. 9, no. 10, pp. 3885–3899, Sep. 2022, doi: 10.1039/d2en00699e.

[21] Y. Su *et al.*, "High-performance piezoelectric composites via β phase programming," *Nat. Commun.*, vol. 13, no. 1, Dec. 2022, doi: 10.1038/s41467-022-32518-3.

[22] X. Li *et al.*, "Unraveling bilayer interfacial features and their effects in polar polymer nanocomposites," *Nat. Commun.*, vol. 14, no. 1, Dec. 2023, doi: 10.1038/s41467-023-41479-0.

[23] S. Bano, B. Gupta, S. K. Sharma, and R. Singh, "Coupling of Triboelectric and Piezoelectric Effects in Nafion-Containing Polyvinylidene Fluoride: Lead Zirconium Titanate Nanofiber-Based Nanogenerators for Self-Powered Systems," *ACS Appl. Nano Mater.*, vol. 7, no. 13, pp. 15425–15437, Jul. 2024, doi: 10.1021/acsanm.4c02292.

[24] P. Kumar, S. Choudhary, K. P. Sharma, S. K. Sharma, and R. Singh, "Light-Sensitive PVDF-TrFE:PDI Hybrid Nanofibers-Based Flexible Bimodal Piezoelectric Nanogenerator," *IEEE Journal on Flexible Electronics*, vol. 1, no. 3, pp. 194–202, Jul. 2022, doi: 10.1109/JFLEX.2022.3189946.

[25] P. Kumar, R. Singh, and S. K. Sharma, "Electrospun P(VDF-TrFE):LiClO4 Hybrid Nanofiber-Based Highly Sensitive Piezocapacitive Pressure Sensors for Self-Powered Flexible Electronics," *ACS Appl. Electron. Mater.*, vol. 7, no. 13, pp. 5821–5831, Jul. 2025, doi: 10.1021/acsaelm.5c00199.

[26] S. Veeralingam and S. Badhulika, "Bi2S3/PVDF/Ppy-Based Freestanding, Wearable, Transient Nanomembrane for Ultrasensitive Pressure, Strain, and Temperature Sensing," Jan. 18, 2021, *American Chemical Society*. doi: 10.1021/acsabm.0c01399.

[27] A. Arrigoni, L. Brambilla, C. Bertarelli, G. Serra, M. Tommasini, and C. Castiglioni, "P(VDF-TrFE) nanofibers: Structure of the ferroelectric and paraelectric phases through IR and Raman spectroscopies," *RSC Adv.*, vol. 10, no. 62, pp. 37779–37796, Oct. 2020, doi: 10.1039/d0ra05478j.

[28] B. Gupta, S. Bano, and R. Singh, "High-performance silver nanoparticles embedded conductive PVA hydrogel for stretchable wearable triboelectric nanogenerators," *J. Power Sources*, vol. 632, Mar. 2025, doi: 10.1016/j.jpowsour.2025.236271.

[29] M. Yang, W. Huang, R. Chen, and Z. Ma, "Flexible Electrospun Nanofibers for Tactile Sensing and Integrated System Research," *IEEE Sens. J.*, vol. 25, no. 1, pp. 9–16, 2025, doi: 10.1109/JSEN.2024.3493072.

[30] S. Dhiman, B. Gupta, S. Bano, and R. Singh, "Temperature-driven soaking of hydrogels for high-performance triboelectric nanogenerators in wearable electronics," *Sens. Actuators A Phys.*, vol. 395, p. 117079, Dec. 2025, doi: 10.1016/j.sna.2025.117079.

[31] S. Ahmad *et al.*, "Enhanced piezoelectric properties of electrospun PVDF nanofibers by integration of ZnO and MgZnO nanoparticles," *Next Materials*, vol. 9, Oct. 2025, doi: 10.1016/j.nxmate.2025.101303.

[32] A. Mondal, M. Faraz, and N. Khare, "Temperature-tuned enhanced performances of PVDF-based flexible triboelectric nanogenerator," *Appl. Phys. Lett.*, vol. 124, no. 10, Mar. 2024, doi: 10.1063/5.0189028.